



UNIVERSIDADE ESTADUAL DE CAMPINAS
SISTEMA DE BIBLIOTECAS DA UNICAMP
REPOSITÓRIO DA PRODUÇÃO CIENTÍFICA E INTELLECTUAL DA UNICAMP

Versão do arquivo anexado / Version of attached file:

Versão do Editor / Published Version

Mais informações no site da editora / Further information on publisher's website:

<https://pubs.rsc.org/-/content/articlelanding/2016/ra/c6ra02027e>

DOI: 10.1039/C6RA02027E

Direitos autorais / Publisher's copyright statement:

©2016 by Royal Society of Chemistry. All rights reserved.

DIRETORIA DE TRATAMENTO DA INFORMAÇÃO

Cidade Universitária Zeferino Vaz Barão Geraldo

CEP 13083-970 – Campinas SP

Fone: (19) 3521-6493

<http://www.repositorio.unicamp.br>



CrossMark
click for updates

Cite this: *RSC Adv.*, 2016, 6, 22213

Au_{1-x}Cu_x colloidal nanoparticles synthesized via a one-pot approach: understanding the temperature effect on the Au : Cu ratio†

Priscila Destro,^a Massimo Colombo,^b Mirko Prato,^b Rosaria Brescia,^b Liberato Manna^b and Daniela Zanchet^{*a}

Gold–copper nanoparticles (Au_{1-x}Cu_x NPs) have been reported as a versatile system to study various aspects related to the colloidal synthesis of bimetallic nanoparticles. In this work, Au_{1-x}Cu_x NPs are synthesized via a one pot approach using equimolar amounts of Au and Cu. Different compositions are obtained by changing the reaction temperature. By taking aliquots at crucial stages of the synthesis and combining several techniques, such as elemental analysis, X-ray diffraction and X-ray photoelectron spectroscopy, it was possible to shed light on the synthesis mechanism: the formation of Au NPs occurs at low temperature, then the higher the synthesis temperature the higher the Cu content in the NPs. In parallel to the Au NPs formation, results of energy-dispersive X-ray spectroscopy analyses carried out in scanning transmission electron microscopy mode suggest the formation of a Cu-rich phase at the early stages of the synthesis. Such a phase, not detectable by X-ray diffraction, acts as a reservoir of Cu species that are slowly released to form the Au_{1-x}Cu_x alloy NPs through a digestive ripening-like process. The reaction temperature and annealing time affect the final Au : Cu ratio but had no significant effect on the final size of the particles, which for all compositions is approximately 14 nm.

Received 22nd January 2016
Accepted 18th February 2016

DOI: 10.1039/c6ra02027e

www.rsc.org/advances

1. Introduction

Advances in the synthesis of nanomaterials have contributed to significant development in fields such as sensors, photonics, drug-delivery systems and, especially, to fulfil the increasing demand for new materials and technologies for energy.^{1,2}

Among the huge variety of nanostructured materials, it is important to highlight the use of metallic nanoparticles (NPs), where the metal confined in a small portion has distinct properties from those of the bulk. In this context, the control of size, shape and composition of the metal NPs represents an important way to obtain new materials for many applications.^{3,4}

The synthesis of gold NPs by colloidal methods has been extensively described using different approaches, enabling accurate control of their properties.^{5,6} The use of Au-based bimetallic NPs has also been presented in the literature as an interesting strategy for the design of new materials.^{7,8} In this context, the AuCu alloy is an interesting example of how the electronic properties of the alloy differ from the simple sum of the properties of Au and Cu.^{9,10} For example, the Au : Cu ratio

reflects directly on the position of the d-band center relative to the Fermi level, which has a strong correlation with the reactivity of materials, especially for applications in catalysis.¹¹ Another point to be featured in the case of the AuCu alloy is the possible formation of chemically ordered alloys. Some metallic nanoparticles such as CoPt,¹² FePt¹³ and AuCo¹⁴ are able to form chemically ordered structures at specific compositions. This ordering can affect different properties of the materials since the distinct symmetry alters the resulting density of states.¹⁵ In the case of AuCu, it is possible to observe chemically ordered alloys of Au₃Cu, AuCu and AuCu₃ compositions.

AuCu NPs can find interest in many fields of applications. Their tunable optical properties, which depend on the shape and composition of NPs, have been explored, for example, in biosensors applications,^{16–18} SERS detection¹⁹ and photothermal therapy,²⁰ showing exciting results. Another important research field in which AuCu NPs have showed interesting and unique properties is heterogeneous catalysis, where supported bimetallic NPs are more active and stable than the monometallic ones.^{21,22}

The study of nanoalloys formation and growth mechanisms has been investigated by different groups because of the applicability of these systems in several areas.^{23–25} Among the methods to obtain nanometric metallic alloys reported in the literature, a widely used strategy is the formation of a metallic seed followed by the incorporation of a second metal, in a two-step growth mechanism.^{26,27} By using a seed of the metal with

^aInstitute of Chemistry, State University of Campinas (UNICAMP), P.O. Box 6154, 13083-970 Campinas, São Paulo, Brazil. E-mail: daniela@iqm.unicamp.br

^bDepartment of Nanochemistry, Istituto Italiano di Tecnologia, Via Morego 30, 16163 Genova, Italy

† Electronic supplementary information (ESI) available. See DOI: 10.1039/c6ra02027e

lowest reduction potential, the second metal can be incorporated by galvanic replacement as nicely explored by Xia and co-workers to produce a large library of nanoalloys starting from Ag seeds.²⁸ In the case of CuAu system, Liu *et al.*²⁹ firstly synthesized Cu NPs, and then by partial replacement of Cu by Au they obtained a Cu@Au core-shell structure. The alloy formation took place by heating the core-shell NPs, through a unidirectional diffusion mechanism in solid state. In a more general case, when the galvanic replacement is not favored, the reduction of the second metal can be done by using a reducing agent. Chen *et al.*³⁰ successfully obtained intermetallic CuAu NPs using Au seeds.

In this work, we explore a one-pot strategy (*i.e.* all reagents are brought into contact at the beginning of the reaction) to synthesize AuCu NPs with different compositions. In this approach, characteristics such as the final size, composition and chemical ordering can be varied by tuning the reaction parameters, *i.e.* metal : metal ratio, metal : ligand ratio and temperature. We produced Au_{1-x}Cu_x spherical NPs of 14 nm in diameter, with a fine control of their composition obtained by optimization of the final reaction temperature; we probed in detail the alloy formation by combining different methods of characterization.

2. Experimental section

2.1 Chemicals

HAuCl₄·3H₂O (99%), and Cu(acac)₂ (99%) were used as metal precursors. Oleylamine (Oley, 70%) and oleic acid (OlAc, 90%) were used as protective agents. 1,2-Hexadecanediol (90%) was used as reducing agent and 1-octadecene (1-ODE, 90%) as solvent. All reactants were purchased from Sigma-Aldrich and used without further purification.

2.2 Synthesis of bimetallic gold-copper NPs

The synthesis of bimetallic AuCu NPs was adapted from the literature.¹⁰ Briefly, 45 mg of HAuCl₄·3H₂O and 30 mg of Cu(acac)₂ (molar ratio Au : Cu 1 : 1) were added to a three-necked round-bottom flask containing 5 mL of 1-ODE, 800 μL of OlAc, 600 μL of Oley and 100 mg of 1,2-hexadecanediol. The mixture was magnetically stirred at room temperature under vacuum for 30 min, generating a green solution. The mixture was heated under vacuum up to 120 °C. After holding at 120 °C for 30 min (step 1), the solution was heated to the final temperature. At about 200 °C, N₂ was fed to the system. The final temperature was set at 225, 260 or 280 °C to obtain different compositions of Au_{1-x}Cu_x NPs (Fig. 1). The reaction was annealed at the corresponding final temperature for 30 min (step 2) and then cooled down. The purification was carried out by adding a toluene : isopropanol (1 : 5 volume ratio) mixture, followed by centrifugation at 4000 rpm for 10 min. Precipitated NPs were dispersed by adding 2 mL of hexane and centrifuged at 2000 rpm for 10 min to remove any undispersed material. This procedure was repeated twice and the particles were then dispersed in hexane. The samples were named based on the final synthesis temperature as AuCu₂₂₅, AuCu₂₆₀ and

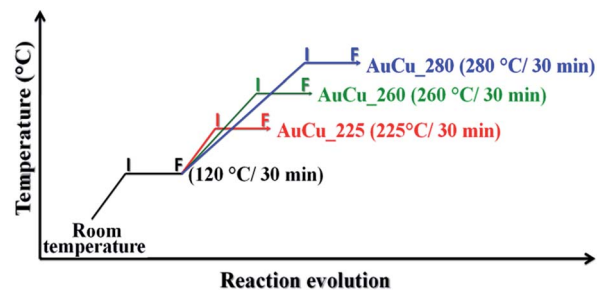


Fig. 1 Heating protocol adopted in the Au_{1-x}Cu_x NPs synthesis. The letters I and F indicate the initial and final points of each step. Step 1 corresponds to 120 °C for 30 min and step 2 to the final temperature for 30 min. See text for more details.

AuCu₂₈₀. To follow the alloy formation, aliquots were taken at different stages of the synthesis, and named by the temperature (100, 120_I, 120_F, 225_I, 225_F, 260_I, 260_F, 280_I, 280_F). The letters I and F indicate, respectively, the beginning and end of steps (1 and 2), on which the temperature was held for 30 min.

2.3 Characterization

Aliquots of approximately 20 μL were collected along the synthesis and diluted in hexane using a quartz cell of 10 mm path length to characterize the Au_{1-x}Cu_x NP growth by UV-Vis analysis, using a Varian Cary 5000 UV-Visible-NIR spectrophotometer in single path configuration within the wavelength range of 200–800 nm with a scanning rate of 10 nm s⁻¹.

Overview bright-field transmission electron microscopy (BF-TEM) analyses were carried out using a JEOL JEM-1011 instrument (thermionic W source, 100 kV high tension). High-angle annular dark field-scanning TEM (HAADF-STEM) analyses were performed using a JEOL JEM-2200FS microscope (Schottky emitter, 200 kV high tension) equipped with a CEOS spherical aberration corrector of the objective lens and an in-column image filter (Ω-type). The shown values for NP diameter and uncertainty were obtained as average and standard deviation over 500 NPs, respectively. Elemental mapping over the Au_{1-x}Cu_x NP samples was carried out by energy-dispersive X-ray spectroscopy (EDS) performed in STEM mode with a Bruker Quantax 400 system with a 60 mm² silicon-drift detector (SDD). The reported elemental maps of Cu and Au were obtained by integration of the Cu Kα and Au Lα after background subtraction and peak deconvolution. For BF-TEM analyses, ~10 μL of the samples were deposited onto carbon-coated Cu grids. For EDS analyses, carbon-coated molybdenum grids and an analytical holder with a Be specimen retainer were used.

The elemental analysis of the colloidal NPs was done by Inductively Coupled Plasma Optical Emission Spectroscopy (ICP) using an iCAP 6000 Thermo Scientific spectrometer. Each sample was obtained by quenching the reaction at the selected temperature, followed by purification. Samples were dissolved in HCl/HNO₃ 3/1 (v/v) overnight, diluted with deionized water (14 μS), and filtered using a PTFE filter before measurement.

The yield of Au and Cu was defined as %_{Metal} and calculated by the eqn (1).

$$\%_{\text{Metal}} = \frac{N_{\text{final}}}{N_{\text{initial}}} \times 100 \quad (1)$$

where %_{Metal} is the final yield of Au or Cu, N_{final} is the molar amount of metal determined by ICP and N_{initial} the molar amount of metal initially added.

X-ray diffraction (XRD) measurements were performed using a Rigaku SmartLab X-ray diffractometer equipped with a 9 kW Cu K α ($\lambda = 1.542 \text{ \AA}$) rotating anode, operating at 40 kV and 150 mA. A zero diffraction silicon substrate was used to collect XRD data on colloidal NPs. The diffraction patterns were collected at room temperature over an angular range of 20–90°, with a step size of 0.05°. XRD data analysis was carried out using PDXL 2.1 software from Rigaku. As for the ICP measurements, each sample was obtained by quenching the reaction at the selected temperature, followed by purification. XRD data were used to estimate the Au_{1-x}Cu_x alloy composition. We used the equation (eqn (2)) proposed by Okamoto *et al.*,³¹ based on experimental values described in the literature for the Au_{1-x}Cu_x solid solution phase with face-centered cubic (fcc) structure:

$$a = 0.40784(1 - x) + 0.36149x + 0.01198x(1 - x) \quad (2)$$

where a is the Au_{1-x}Cu_x lattice parameter and x is the copper atomic fraction, defined as $N_{\text{Cu}}/(N_{\text{Cu}} + N_{\text{Au}})$, where N_x is the number of atoms of the element x . Since the Au_{1-x}Cu_x alloy system shows a positive deviation from the Vegard's law, the equation proposed by Okamoto *et al.*³¹ gives a more accurate estimation of the alloy composition.

X-ray photoelectron spectroscopy (XPS) measurements were performed on a Kratos Axis Ultra DLD spectrometer, using a monochromatic Al K α source (15 kV, 20 mA). Wide scans were acquired at an analyzer pass energy of 160 eV. High-resolution narrow scans were performed at constant pass energy of 10 eV and steps of 0.1 eV. Photoelectrons were detected at a takeoff angle of $\Phi = 0^\circ$ with respect to the surface normal. The pressure in the analysis chamber was maintained below 7×10^{-9} Torr for data acquisition. The samples were prepared by drop-casting a few microliters of purified NPs solutions onto a graphite substrate (HOPG, ZYB quality, NTMDT), which was then transferred to the XPS setup. Data were converted to VAMAS format and processed using CasaXPS 2.3.16 software. The binding energy scale was internally referenced to the C 1s peak (BE for C–C = 285 eV). Semi-quantitative analysis was performed by measuring the areas under selected Au and Cu XPS peaks and by applying appropriate atomic sensitivity factors, as obtained by the instrument manufacturer.

3. Results

Au and Cu NPs exhibit a characteristic absorption band in the visible region due to plasmon excitation.³² Plasmon band arises from the collective oscillation of the free electrons induced by the interaction with visible light.³³ While Au NPs characteristic plasmon band is centered at approximately 520 nm, the Cu NPs

plasmon appears at 560 nm, and the Au_{1-x}Cu_x NPs alloy plasmon is observed between these two values.¹⁰ For this reason, we firstly followed the evolution of synthesis products by UV-Vis spectroscopy, as shown in Fig. 2. At 100 °C (black lines in Fig. 2a–c) the characteristic plasmon resonance of Au NPs is observed around 520 nm, indicating that the formation of Au NPs already occur before reaching this temperature. In fact, around 70 °C the color of the solution changes from orange to deep red and TEM images at 100 °C confirm the formation of NPs (Fig. S1a†). By increasing the temperature, it is possible to observe a similar profile at 120 °C in all the three tests performed. Above this temperature, a red shift occurs and the plasmon peak becomes asymmetric, indicating the incorporation of copper into the Au NPs. Among the samples, the red shift increases as a function of final temperature: AuCu₂₂₅ shows a plasmon band at 540 nm (Fig. 2a), AuCu₂₆₀ at 550 nm (Fig. 2b) and AuCu₂₈₀ at 552 nm (Fig. 2c). In contrast, there is no significant change in the peak width, indicating that the NPs remain stable by the incorporation of Cu.³⁴

Fig. 3 shows the BF-TEM images and corresponding size distribution histograms of the final particles. According to the BF-TEM analyses, the AuCu₂₂₅ sample shows spherical and uniform NPs, with a diameter of 14 ± 1 nm. Despite small variations from batch to batch, the average particle size did not significantly change with the reaction temperature: we measured 13 ± 1 nm for AuCu₂₆₀ and 14 ± 1 nm for AuCu₂₈₀. For AuCu₂₆₀, it is possible to observe also some less isotropic particles, which become the dominant population for the AuCu₂₈₀ sample. The lower isotropy in these samples may be due to a structural rearrangement upon incorporation of a higher fraction of Cu atoms in the initial Au structure and/or to the higher final temperature.

Elemental analysis by ICP was performed on the final products and on all the aliquots collected during the syntheses to get

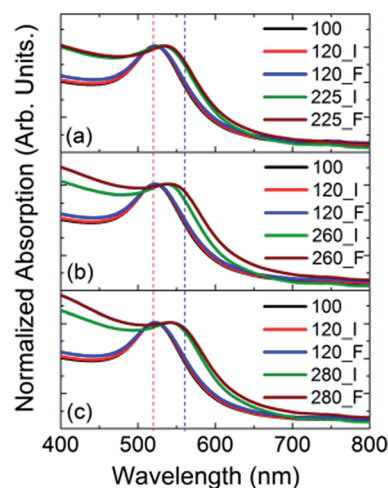


Fig. 2 UV-Vis spectra following the Au_{1-x}Cu_x NPs synthesis at different final temperatures: (a) AuCu₂₂₅, (b) AuCu₂₆₀ and (c) AuCu₂₈₀. The red dashed line indicates the position of Au plasmon and the blue dashed line the Cu plasmon position.

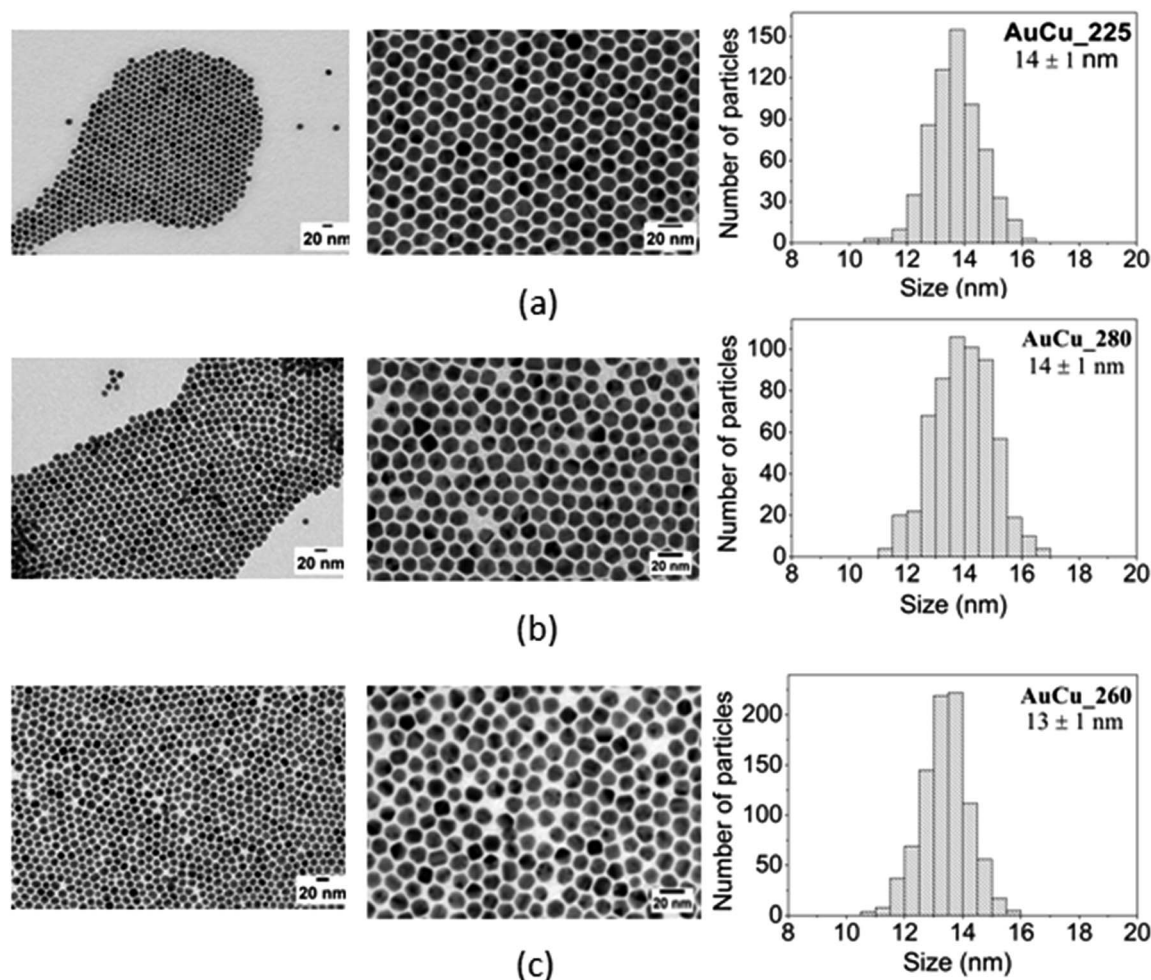


Fig. 3 BF-TEM images and size distribution of (a) AuCu₂₂₅, (b) AuCu₂₆₀ and (c) AuCu₂₈₀.

more information about the growth mechanism of the Au_{1-x}Cu_x NPs. The results are presented in Table 1.

ICP values for 100, 120_I and 120_F aliquots are common for the three syntheses. It is possible to verify that around 100 °C, only a small amount of Cu is detected in the final product, reaching 22% after 30 min at 120 °C. This is about 44% of the Cu added at the beginning of reaction. In line with UV-Vis spectroscopy data, the increase of the synthesis final temperature results in higher amounts of copper in the final product, going from 24.5% at 225 °C up to 48.8% at 280 °C. The annealing time at the final temperature is also important to increase the Cu incorporation. This is evident especially for the AuCu₂₆₀ and AuCu₂₈₀ samples, where an increase of the copper content of about 11% is found with the annealing. It is interesting to mention that the yield of Au is also affected by the final temperature, decreasing from 40% in case of the AuCu₂₂₅ sample, to 20% for AuCu₂₈₀. At a given temperature, longer annealing increases further the Cu fraction in the final product, but the yield of the synthesis decreases considerably. The dependence of the yield with time and temperature can be related to an increased collision of the formed particles, forming larger aggregates that were removed in the purification

step and/or to a poor stability of the NPs with higher content of copper. Attempts to form Cu enriched alloy NPs, such as Au_{0.25}Cu_{0.75} by changing the amount of Cu added at the beginning of the synthesis failed under these synthesis conditions. It is worth to point out that other authors report the formation of Au_{0.25}Cu_{0.75} NPs³⁰ and Au_{0.33}Cu_{0.77} (ref. 34) using different conditions, but the yields were not reported.

Table 1 Cu (at%) at different temperatures by ICP

Temperature	Sample		
	AuCu ₂₂₅	AuCu ₂₆₀	AuCu ₂₈₀
100 ^a	9.4		
120_I ^a	14.3		
120_F ^a	22.3		
225_I	31.6		
225_F	24.5	—	—
260_I	—	27.7	—
260_F	—	37.8	—
280_I	—	—	36.1
280_F	—	—	48.8

^a Common steps for the three samples.

Table 2 shows the quantitative XPS results, wherein the amount of Cu increases with temperature. Interestingly, although XPS is a surface technique, probing a few atomic layers (<2 nm for Cu and Au),³⁵ it shows Cu at% similar to those measured by ICP. These results indicate a homogeneous distribution of both metals in the synthesis product, at all stages, ruling out the formation of a core-shell structure with, for example, a Cu-rich shell. However, it is important to note that a similar result could also be found, for example, if Au and Cu single-metal particles were formed. This hypothesis is excluded by STEM-EDS mapping over individual particles (see Fig. S2†), showing a homogeneous distribution of both metals in the NPs.

The amount of Cu that was effectively alloyed with Au was quantified by XRD analyses. Both metals exhibit a fcc structure, and the variation in lattice parameter is related to the Au : Cu ratio in the alloy (eqn (2)).³¹ Fig. 4 shows the corresponding diffractograms in which a clear shift of the peak positions can be seen as the synthesis proceeds. The dashed lines in Fig. 4 correspond to the (111) peak position of metallic Au ($a = 4.08 \text{ \AA}$, red line) and metallic Cu ($a = 3.61 \text{ \AA}$, blue line). It can be seen that during the first reaction step (120 °C), common to all samples, XRD confirms the formation of monometallic Au NPs, in agreement with the UV-Vis results. By increasing the temperature, the peak positions shift to larger Bragg angle values showing a decrease of the lattice parameter in agreement with the incorporation of Cu into the Au lattice. The results also show that the higher the temperature, the larger the shift, indicating higher Cu incorporation. Interestingly, in the case of AuCu_280 sample the superlattice peaks related to the chemically ordered tetragonal structure of AuCu can also be seen.³⁶ Therefore, although the yield of NPs decreases with temperature and annealing time, keeping the system at 280 °C for 30 min lead to NPs with Au : Cu molar ratio of 1 : 1, matching the initial metals ratio, and favoring the formation of the chemically ordered bimetallic AuCu phase.

Table 3 presents the Cu at% obtained by the analysis of the lattice parameter. It is possible to confirm the increase in the copper amount as a function of the temperature, similarly to what was observed by ICP and XPS analyses. However, while ICP/XPS showed that the total amount of Cu raises steadily, *e.g.*

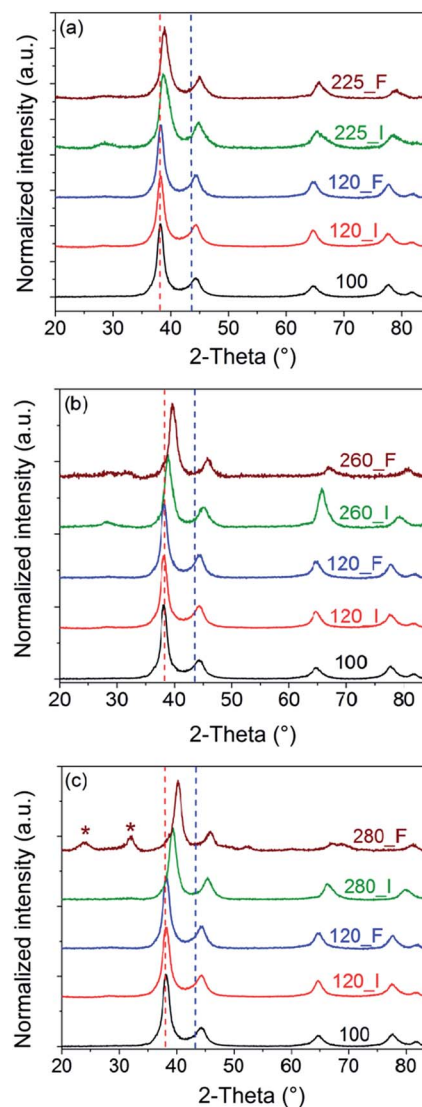


Fig. 4 XRD patterns of $\text{Au}_{1-x}\text{Cu}_x$ NPs at different stages of the synthesis: (a) AuCu_225, (b) AuCu_260 and (c) AuCu_280. The red dashed line indicates the (111) peak position of Au ($a = 4.08 \text{ \AA}$, JCPDS no. 00-004-0784) and the blue one indicates the (111) position of Cu ($a = 3.61 \text{ \AA}$, JCPDS no. 00-901-3023). The superlattice peaks of the chemically ordered AuCu phase (JCPDS no. 01-071-5026) are indicated by * in (c).

Table 2 Cu (at%) at different temperatures obtained by XPS

Temperature	Sample		
	AuCu_225	AuCu_260	AuCu_280
100 ^a	3.4	—	—
120_I ^a	5.7	—	—
120_F ^a	22.3	—	—
225_I	29.5	—	—
225_F	26.5	—	—
260_I	—	28.6	—
260_F	—	40.3	—
280_I	—	—	36.2
280_F	—	—	40.4

^a Common steps for the three samples.

from about 10% when reaching 120 °C (120_I) up to 20% after 30 min at this temperature (120_F), XRD gives no indication that the Cu is incorporated in the Au lattice at this temperature. In all stages, the Cu contents found by XRD are smaller than those measured by ICP/XPS, with the exception of the final stages at 260 °C (260_F) and 280 °C (280_F).

Fig. 5 compares the results found by ICP and XRD. It is possible to observe that, as the syntheses proceed, the values obtained by the two techniques tend to converge toward the same values. These results likely indicate that part of the Cu species present at the beginning of the synthesis, which precipitate together with the Au NPs during the purification process, are not detectable by XRD, not even as a separate phase (*e.g.* metallic Cu or crystalline copper oxides).

Table 3 Cu (at%) derived from the lattice parameter, obtained by XRD (eqn (1))

Temperature	Sample		
	AuCu_225	AuCu_260	AuCu_280
100 ^a	0		
120_I ^a	0		
120_F ^a	0		
225_I	15.0		
225_F	19.2	—	—
260_I	—	21.9	—
260_F	—	38.1	—
280_I	—	—	30.1
280_F	—	—	50.0

^a Common steps for the three samples.

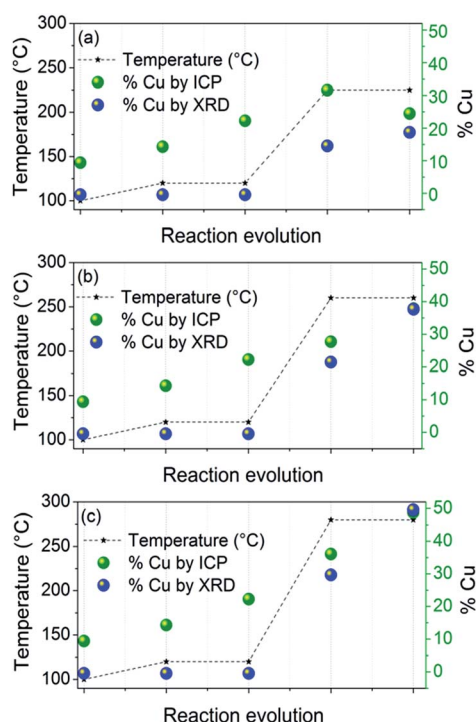


Fig. 5 Comparison of the Cu (at%) obtained by ICP and XRD as a function of the synthesis temperature of (a) AuCu₂₂₅, (b) AuCu₂₆₀ and (c) AuCu₂₈₀.

In order to understand this difference, a detailed analysis was performed by HAADF-STEM imaging and STEM-EDS elemental analysis on samples 280_I and 280_F as shown in Fig. 6 and S2.† Besides the high-contrast (*i.e.*, high thickness and/or mean atomic number) of the Au_{1-x}Cu_x NPs, a fainter contrast region can be observed in HAADF-STEM images around the particles for the sample 280_I, as indicated by arrows in Fig. 6. This region is mainly composed by copper, as shown by the corresponding STEM-EDS analysis. Although this type of analysis is local, this result, associated to the similar quantification of Au and Cu provided by ICP and XPS, is strong evidence that the reduction of Cu leads initially to the

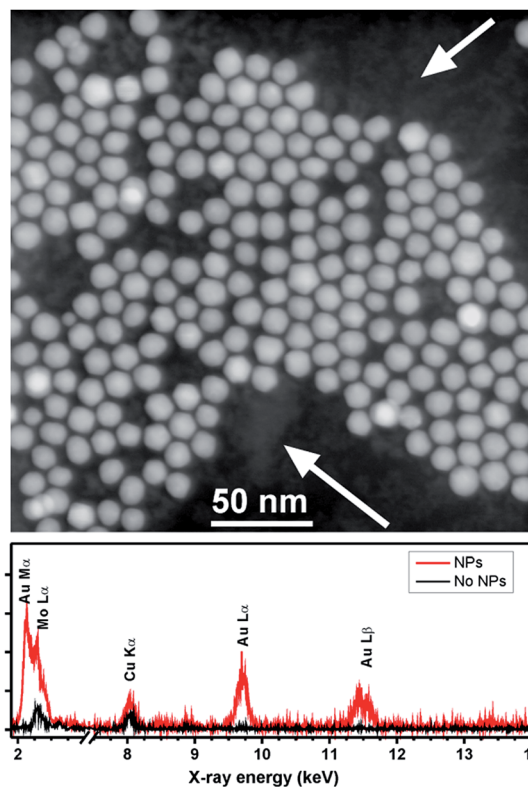


Fig. 6 HAADF-STEM image of 280_I sample, showing the presence of a lower contrast phase (indicated by arrows) surrounding the Au_{1-x}Cu_x NPs, mainly composed by copper as demonstrated by the comparison between STEM-EDS spectra collected on NPs and on the surrounding phase (identical area and acquisition time).

formation of a Cu-rich phase that cannot be identified by means of XRD.

4. Discussion

In the one-pot synthetic method, both metals precursors are added together to the initial solution and, depending on the reaction conditions, one may expect the formation of an alloy already in the early stages of the synthesis process. Previous works in the Au_{1-x}Cu_x system found, however, that in fact Au nucleates first.^{10,37} Destro *et al.*³⁸ probed the formation of the AuCu alloy (in air) by *in situ* X-ray absorption fine structure spectroscopy (XAFS) and confirmed that Au reduction starts already at 70 °C. In the present work, where the synthesis was performed in vacuum/inert atmosphere, the results confirmed that Au precursor is reduced first, and alloy formation is highly dependent on the temperature. Considering the experimental conditions implemented in the present work, the early reduction of Au can be rationalized considering that 1,2-hexadecanediol is not a strong reducing agent, in particular at low temperature, and that Au³⁺ is reduced easier than Cu²⁺ due to the higher reduction potential (+1.5 and +0.3 eV respectively).³⁹

One interesting consequence of the formation of mono-metallic Au NPs at the early stages of the synthesis is that the Au_{1-x}Cu_x NPs, characterized by different compositions, show

similar sizes. This is in agreement with the results reported by Motl *et al.*;⁴⁰ they implemented a one-pot synthesis approach where the amount of Cu in the NPs was controlled by the Au : Cu ratio of the precursors. They analyzed eight samples with copper contents ranging from 0 to 50 (at%) and seven of them showed an average size in the 10–13 nm range. Recently, Sinha *et al.*,³⁷ explored the one-pot strategy for the synthesis of $Au_{1-x}Cu_x$ NPs by varying the (Oley + OlAc)/metal and Oley/OlAc ratios seeking to control the average particles size. They reported that a 40 : 1 total ligand : metal ratio led to the smallest average size of the NPs (*i.e.* about 14 nm). This value is in line with our results, where the total ligand : metal ratio is 50 : 1. According to Sinha *et al.*,³⁷ it was not possible to decrease the particle size below this value just by increasing the amount of ligands. Smaller $Au_{1-x}Cu_x$ NPs were only obtained by using a seed mediated approach where pre-formed Au NPs are added to solution containing the copper precursor.³⁰ We have also found similar results, where the final temperature of the synthesis impact both the Au : Cu ratio and the eventual chemical order of the alloy without affecting significantly the average particles size. In fact, at 100 °C when most of the Au ions have already been reduced forming the NPs, the mean size is 14 nm (see Fig. S1†). It is worth to point out that the increase of the Cu content in the NPs from 25% (AuCu_{0.225}) to 50% (AuCu_{0.280}) should lead to an increase of about 11% in size. This small increase would be hardly detected by TEM due to the size distribution of the particles. Different parameters such as total ligand/metal ratio, heating ramp and temperature of step 1 were also varied but did not impact significantly in the final particle size (results not reported).

More interestingly, how the Cu atoms are generated and incorporated to form the alloy is still not clear and there are some possible mechanisms that can lead to the $Au_{1-x}Cu_x$ alloy formation. Chen *et al.*³⁰ proposed that in the seed mediated synthesis, a diffusion-based mechanism takes place. They proposed that Cu^{2+} ions were reduced to Cu atoms and/or small cluster in solution. Then, by colliding with the Au NPs Cu species diffuses into the core of the NPs forming the alloy. No evidence of a core-shell structure was found. On the other hand, Shore *et al.*⁴⁰ observed a core-shell structure in AuAg system at low temperature (<200 °C) and the alloy formation was achieved by increasing the temperature. They also showed that similar AuAg alloy NPs could be directly obtained by heating Au NPs in the presence of Ag precursor at higher temperatures (~250 °C).

In our work, the combination of XPS, ICP, TEM, XRD and STEM-EDS does not indicate the formation of a core-shell structure or the direct formation of atomic species of copper that would collide and diffuse into the Au NPs. We showed that the Au NPs are formed at low temperature and that the amount of Cu in the final product progressively increases with the reaction temperature. Moreover, the copper content inferred from XRD analysis was systematically smaller than that measured by ICP and XPS at all reaction stages except at the end of the annealing step. Our results strongly indicate that a Cu-rich phase, undetectable by XRD, was initially formed and then progressively digested in the reaction medium at high temperatures. This Cu phase, amorphous or formed by few nm-sized Cu or CuO_x nanocrystals, acts as a reservoir of Cu species

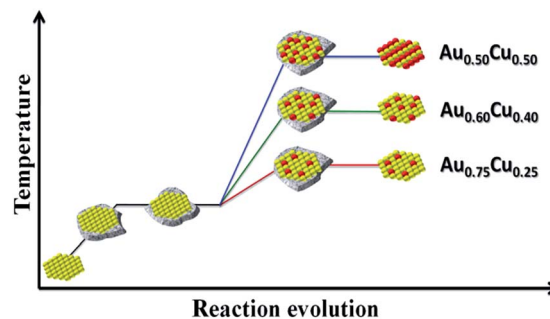


Fig. 7 Proposed growth mechanism of $Au_{1-x}Cu_x$ alloy NPs. Yellow = Au atom, red = Cu atom, gray = solid Cu-rich phase.

that are released as the synthesis proceeds and that are incorporated into the Au NPs through a solid state diffusion process.

The growth mechanism of our $Au_{1-x}Cu_x$ NPs resembles the mechanism called digestion ripening described by Smetana *et al.*⁴¹ in which AuCu and AuAg alloy NPs were obtained by mixing and heating preformed single metal colloidal NPs in the presence of alkanethiol under reflux. This mechanism is highly dependent on the ligand and temperature, and core-shell NPs have also been prepared by this method at lower temperatures.^{42–44} We speculate that the large excess of ligands and the high temperature achieved in our synthesis can promote the digestion of the Cu-rich phase leading to the formation of the $Au_{1-x}Cu_x$ alloy, as proposed in Fig. 7.

It is interesting to note that we did not find indication of the formation of core-shell Au@Cu NPs in any stage of the synthesis (Fig. S1†). Recently, Liu *et al.*²⁹ studied Cu@Au NPs and nicely proposed the formation of CuAu alloy through a unidirectional diffusion route of Au atoms into to Cu core. The driving force for the Au diffusion was proposed to be the structural disorder of the shell, enhanced by temperature. The unidirectional diffusion mechanism was associated instead to the structural stability of an Au-diluted CuAu alloy front. In our case, since Au NPs formed first, we could expect initially the formation of Au@Cu NPs that would then be converted to $Au_{1-x}Cu_x$ alloy. This would happen if enough copper species were available in solution at low temperatures and metal diffusivities were limiting the alloy formation. In fact, Destro *et al.*³⁸ showed by *in situ* XAFS that the reduction of copper starts already at about 120 °C. As a consequence, our results suggest that the digestion of a Cu-rich phase forming species available in solution is the limiting factor, and the temperature controls the final composition of the $Au_{1-x}Cu_x$ NPs.

The possibility of an accurate composition control by the colloidal method keeping the same size distribution is an interesting and useful approach for several applications, for example in heterogeneous catalysis,²² since it makes possible to analyze the effect of the alloy composition using particles of similar size and shape.

5. Conclusions

We evaluated the effect of the temperature on the synthesis of $Au_{1-x}Cu_x$ alloy colloidal NPs *via* one-pot approach. By changing

the final reaction temperature it was possible to obtain uniform spherical particles, with size of about 14 nm, with different composition: Au_{0.75}Cu_{0.25} at 225 °C, Au_{0.60}Cu_{0.40} at 260 °C and Au_{0.50}Cu_{0.50} at 280 °C. By combining different techniques, it was possible to propose a growth mechanism, where Au NPs are formed at low temperatures together with a Cu-rich phase. This intermediary Cu-rich phase acts as a reservoir of Cu atoms that are incorporated into the Au NPs at a given temperature through a digestive ripening like-process.

The results presented here clearly point out the important role played by the temperature in the formation of bimetallic Au_{1-x}Cu_x NPs. Despite the efforts, we still lack deeply studies on the phase diagrams at nanoscale, as well as the main mechanisms that determine atomic diffusion and phase segregation at nanoscale. This is of crucial importance in several areas, such as catalysis, where the interaction with supports and reaction medium can further affect the stability of nanoalloys. We hope that our results will contribute to motivate further theoretical and experimental studies in this direction.

Acknowledgements

We acknowledge São Paulo Research Foundation (FAPESP, 2011/50727-9) for financial support and Brazilian Nanotechnology National Laboratory (LNNano) for the access to electron microscopy facilities at the beginning of this work. PD acknowledges Conselho Nacional de Desenvolvimento Científico e Tecnológico (CNPq, 870359/1997-5) and Coordenação de Aperfeiçoamento de Pessoal de Nível Superior-Science Without Borders Program (CAPES, 99999.013076/2013-02) for fellowships. DZ acknowledges CNPq for financial support (306242/2010-4 and 309373/2014-0).

References

- 1 N. Toshima and T. Yonezawa, *New J. Chem.*, 1998, **22**, 1179–1201.
- 2 S. Jana, *Dalton Trans.*, 2015, **44**, 18692–18717.
- 3 K. J. Major, C. De and S. O. Obare, *Plasmonics*, 2009, **4**, 61–78.
- 4 A. K. Singh and Q. Xu, *ChemCatChem*, 2013, **5**, 652–676.
- 5 M. Brust, M. Walker, D. Bethell, D. J. Schiffrin and R. Whyman, *Chem. Commun.*, 2000, 801–802.
- 6 R. Sardar, A. M. Funston, P. Mulvaney and R. W. Murray, *Langmuir*, 2009, **25**, 13840–13851.
- 7 C. J. DeSantis, R. G. Weiner, A. Radmilovic, M. M. Bower and S. E. Skrabalak, *J. Phys. Chem. Lett.*, 2013, **4**, 3072–3082.
- 8 A. K. Sra and R. E. Schaak, *J. Am. Chem. Soc.*, 2004, 6667–6672.
- 9 G. Barcaro, A. Fortunelli, G. Rossi, F. Nita and R. Ferrando, *J. Phys. Chem. B*, 2006, **110**, 23197–23203.
- 10 N. E. Motl, E. Ewusi-annan, I. T. Sines, L. Jensen and R. E. Schaak, *J. Phys. Chem.*, 2010, **114**, 19263–19269.
- 11 D. Kim, J. Resasco, Y. Yu, A. M. Asiri and P. Yang, *Nat. Commun.*, 2014, **5**, 1–8.
- 12 D. Alloyeau, C. Ricolleau, C. Mottet, T. Oikawa, C. Langlois, Y. Le Bouar, N. Braidly and A. Loiseau, *Nat. Mater.*, 2009, **8**, 940–946.
- 13 S. Sun, C. B. Murray, D. Weller, L. Folks and A. Moser, *Science*, 2000, **287**, 1989–1992.
- 14 K. A. Kuttiyiel, K. Sasaki, D. Su, L. Wu, Y. Zhu and R. R. Adzic, *Nat. Commun.*, 2014, **5**, 1–8.
- 15 V. V. Nemoshkalenko, K. V. Chuistov, V. G. Aleshin and A. I. Senkevich, *J. Electron Spectrosc. Relat. Phenom.*, 1976, **9**, 169–173.
- 16 S. Y. Tee, E. Ye, P. H. Pan, C. J. J. Lee, H. K. Hui, S.-Y. Zhang, L. D. Koh, Z. Dong and M.-Y. Han, *Nanoscale*, 2015, **7**, 11190–11198.
- 17 L. Y. Chen, T. Fujita, Y. Ding and M. W. Chen, *Adv. Funct. Mater.*, 2010, **20**, 2279–2285.
- 18 S.-I. Kim, G. Eom, M. Kang, T. Kang, H. Lee, A. Hwang, H. Yang and B. Kim, *Nanotechnology*, 2015, **26**, 2–9.
- 19 Z. Jiang, Q. Zhang, C. Zong, B.-J. Liu, B. Ren, Z. Xie and L. Zheng, *J. Mater. Chem.*, 2012, **22**, 18192–18197.
- 20 R. He, Y. Wang, X. Wang, Z. Wang, G. Liu, W. Zhou, L. Wen, Q. Li, X. Wang, X. Chen, J. Zeng and J. G. Hou, *Nat. Commun.*, 2014, **5**, 1–10.
- 21 C. L. Bracey, P. R. Ellis and G. J. Hutchings, *Chem. Soc. Rev.*, 2009, **38**, 2231–2243.
- 22 S. Najafshirtari, R. Brescia, P. Guardia, S. Marras, L. Manna and M. Colombo, *ACS Catal.*, 2015, **5**, 2154–2163.
- 23 L. Zhang, W. Niu and G. Xu, *Nano Today*, 2012, **7**, 586–605.
- 24 H. You, S. Yang, B. Ding and H. Yang, *Chem. Soc. Rev.*, 2013, **42**, 2880–2904.
- 25 R. Ferrando, J. Jellinek and R. L. Johnston, *Chem. Rev.*, 2008, **108**, 845–910.
- 26 L. Au, X. Lu and Y. Xia, *Adv. Mater.*, 2008, **20**, 2517–2522.
- 27 G. D. Moon, S. Ko, Y. Min, J. Zeng, Y. Xia and U. Jeong, *Nano Today*, 2011, **6**, 186–203.
- 28 Y. Xia, Y. Xiong, L. Byungkwon and S. E. Skrabalak, *Angew. Chem.*, 2009, **48**, 60–103.
- 29 S. Liu, Z. Sun, Q. Liu, L. Wu, Y. Huang, T. Yao and J. Zhang, *ACS Nano*, 2014, **8**, 1886–1892.
- 30 W. Chen, R. Yu, L. Li, A. Wang, Q. Peng and Y. Li, *Angew. Chem.*, 2010, **122**, 2979–2983.
- 31 H. Okamoto, D. J. Chakrabarti, D. E. Laughlin and T. B. Massalski, *Bull. Alloy Phase Diagrams*, 1987, **8**, 454–473.
- 32 Z. A. Bansal, J. S. Sekhon and S. S. Verma, *Plasmonics*, 2013, **9**, 143–150.
- 33 J. M. Romo-Herrera, R. a. Alvarez-Puebla and L. M. Liz-Marzán, *Nanoscale*, 2011, **3**, 1304–1315.
- 34 Z. Xu, E. Lai, Y. Shao-Horn and K. Hamad-Schifferli, *Chem. Commun.*, 2012, **48**, 5626–5628.
- 35 S. Tanuma, C. J. Powell and D. R. Penn, *Surf. Interface Anal.*, 2000, **21**, 165–176.
- 36 R. E. Schaak, A. K. Sra, B. M. Leonard, R. E. Cable, J. C. Bauer, Y.-F. Han, J. Means, W. Teizer, Y. Vasquez and E. S. Funck, *J. Am. Chem. Soc.*, 2005, **127**, 3506–3515.
- 37 S. K. Sinha, C. Srivastava, S. Sampath and K. Chattopadhyay, *RSC Adv.*, 2015, **5**, 4389–4395.
- 38 P. Destro, D. Cantane, G. Honorio, L. Costa, D. Meira and D. Zanchet, under preparation.
- 39 F. Gauthard, F. Epron and J. Barbier, *J. Catal.*, 2003, **220**, 182–191.

- 40 M. S. Shore, J. Wang, A. C. Johnston-Peck, A. L. Oldenburg and J. B. Tracy, *Small*, 2011, **7**, 230–234.
- 41 A. B. Smetana, K. J. Klabunde, C. M. Sorensen, A. A. Ponce and B. Mwale, *J. Phys. Chem. B*, 2006, **110**, 2155–2158.
- 42 S. P. Bhaskar, M. Vijayan and B. R. Jagirdar, *J. Phys. Chem. C*, 2014, **118**, 18214–18225.
- 43 S. B. Kalidindi and B. R. Jagirdar, *J. Phys. Chem. C*, 2008, **112**, 4042–4048.
- 44 D. Jose and B. R. Jagirdar, *J. Phys. Chem. C*, 2008, **112**, 10089–10094.